# Bioinspired Exosome-Mimetic Nanovesicles for Targeted Delivery of Chemotherapeutics to Malignant Tumors

**Su Chul Jang,[†] Oh Youn Kim,[†] Chang Min Yoon,[†] Dong-Sic Choi,[†] Tae-Young Roh,[†] Jaesung Park,[‡] Jonas Nilsson,[§] Jan Lötvall,[⊥] Yoon-Keun Kim,[†] and Yong Song Gho[†,*]**

[†]Department of Life Sciences, Pohang University of Science and Technology, Pohang, Gyeongbuk 790-784, Republic of Korea, [‡]Department of Mechanical Engineering, Pohang University of Science and Technology, Pohang, Gyeongbuk 790-784, Republic of Korea, [§]Department of Clinical Chemistry and Transfusion Medicine, Institute of Biomedicine, The Sahlgrenska Academy, University of Gothenburg, Sahlgrenska University Hospital, Gothenburg 413 45, Västergötland, Sweden, and [⊥]Krefting Research Center, Department of Internal Medicine, Institute of Medicine, The Sahlgrenska Academy, University of Gothenburg, Gothenburg 405 30, Västergötland, Sweden

**ABSTRACT** Exosomes, the endogenous nanocarriers that can deliver biological information between cells, were recently introduced as new kind of drug delivery system. However, mammalian cells release relatively low quantities of exosomes, and purification of exosomes is difficult. Here, we developed bioinspired exosome-mimetic nanovesicles that deliver chemotherapeutics to the tumor tissue after systemic administration. The chemotherapeutics-loaded nanovesicles were produced by the breakdown of monocytes or macrophages using a serial extrusion through filters with diminishing pore sizes (10, 5, and 1 $\mu$m). These cell-derived nanovesicles have similar characteristics with the exosomes but have 100-fold higher production yield. Furthermore, the nanovesicles have natural targeting ability of cells by maintaining the topology of plasma membrane proteins. *In vitro*, chemotherapeutic drug-loaded nanovesicles induced TNF-$\alpha$-stimulated endothelial cell death in a dose-dependent manner. *In vivo*, experiments in mice showed that the chemotherapeutic drug-loaded nanovesicles traffic to tumor tissue and reduce tumor growth without the adverse effects observed with equipotent free drug. Furthermore, compared with doxorubicin-loaded exosomes, doxorubicin-loaded nanovesicles showed similar *in vivo* antitumor activity. However, doxorubicin-loaded liposomes that did not carry targeting proteins were inefficient in reducing tumor growth. Importantly, removal of the plasma membrane proteins by trypsinization eliminated the therapeutic effects of the nanovesicles both *in vitro* and *in vivo*. Taken together, these studies suggest that the bioengineered nanovesicles can serve as novel exosome-mimetics to effectively deliver chemotherapeutics to treat malignant tumors.

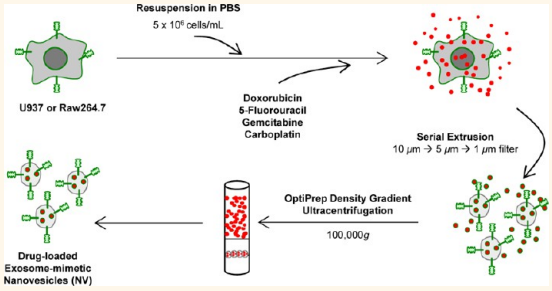


**KEYWORDS:** exosome-mimetics · exosomes · extracellular vesicles · biomimicry · drug delivery systems

Genetic instability is a hallmark of the transformation of normal cells to become a malignant cell.[1] By enabling the accumulation of mutations and chromosomal aberrations, the cells can activate signaling pathways leading to tumor progression. However, hyper-activated growth signaling initially results in oncogenic stress, which is detected at the cell cycle checkpoints.[2] Therefore, for tumors to develop, tumor suppressor genes regulating cell cycle checkpoints are lost by mutation. Classical chemotherapeutic drugs work by inducing DNA damage either directly or indirectly.[3] Normal cells can respond to this by inducing a DNA damage response, which results in cell cycle arrest. Tumor cells, on the other hand, have disrupted their cell cycle checkpoints during tumorigenesis and cannot produce a prolonged cell cycle arrest.[4] This results in the progression of the cell cycle with damaged DNA, which results in tumor cell death. Therefore, a small therapeutic window exists whereby the tumor cells are more sensitive to chemotherapy than normal cells. On the other hand, prolonged or too aggressive treatment often results in damage to normal cells of the intestine, skin, and the hematopoietic system.[5] This limits the efficacy of classic cytostatic drugs and results in poor overall survival of patients with solid tumors. Therefore, methods

* Address correspondence to ysgho@postech.ac.kr.

Received for review May 3, 2013 and accepted August 28, 2013.

**Published online August 28, 2013**
**10.1021/nn402232g**

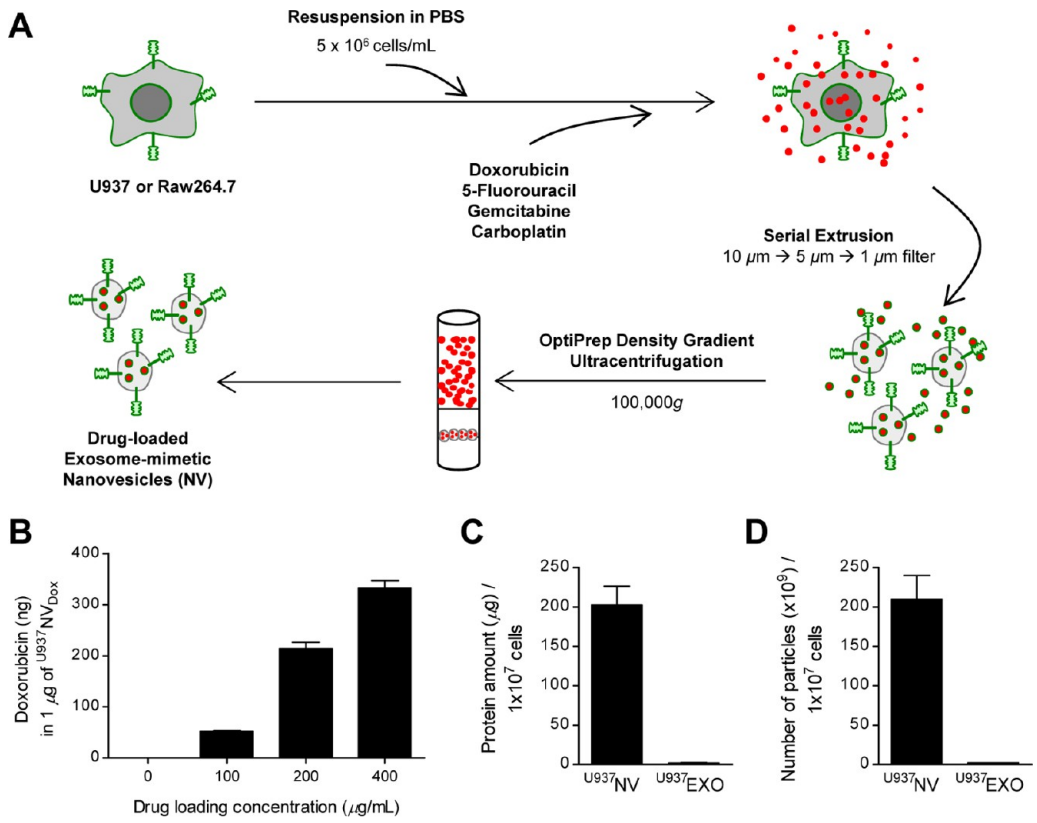


**Figure 1. Generation of exosome-mimetic nanovesicles (NV) and chemotherapeutics-loaded NV. (A) Schematic illustration of the procedure for the generation of NV and chemotherapeutics-loaded NV. (B) Quantification of doxorubicin packaged into $^{U937}NV_{Dox}$ when 100, 200, or 400 $\mu$g/mL of doxorubicin was used in the cell suspension solution ($n$ = 3 per dose). (C,D) The yields of $^{U937}$NV and $^{U937}$EXO measured as the total protein (C) and particle number (D) from 1 $\times$ $10^7$ U937 cells ($n$ = 3, respectively). EXO: exosomes.**

decreasing systemic toxicity would improve treatments for cancer patients.

One way of achieving reduced side effects is to target delivery of the anticancer drug to the tumor. Encapsulating the drug in a tumor targeting vehicle or making a pro-drug that is specifically activated in the lineage of the cancer cell could achieve this. In the former case, significant efforts have been made to develop nanotechnology for well-designed targeted drug delivery system.[6−8] Various types of nanocarriers such as liposomes, nanoparticles, and polymeric particles have been fabricated from various materials.[9−11] Nanocarriers have several advantages in drug delivery: high payload of drugs, multiple drug loading, protection from drug degradation, and enhancement of endocytosis.[12] Moreover, nanocarriers are especially potent in tumor treatment in that they achieve passive targeting *via* enhanced permeability and retention effect on leaky vasculature of tumors.[13] However, issues related to their artificial nature can limit their effects and cause toxicology issues.[14]

In the present study, we have used our knowledge on the naturally released nanosized extracellular vesicles called exosomes to develop a method for safe and efficient delivery system for cytotoxic drugs. Mammalian cells actively release exosomes that have diameters of 40−150 nm.[15,16] Exosomes contain various proteins and RNAs that have many regulatory effects on recipient cells.[17−22] Exosomes can deliver their cargo to other cells and can thereby change the phenotype of the recipient cells. The multiple physiological roles of exosomes in intercellular communication can be explained by their ability to carry genetic and proteomic information between cells.[17−22] Moreover, because exosomes are nanosized and carry cell surface molecules, they have a high capacity for penetrating the interstitia of organs as well as a natural targeting capacity.[23−26] However, most mammalian cells release relatively low quantities of exosomes and purification of exosomes is cumbersome, which results in a relatively low yield.[27,28] Therefore, the generation of exosome-mimetic vesicles with a substantially greater yield is attractive for the development of future nanosized drug delivery systems.

Here we developed bioengineered and bioinspired cell-derived nanocarriers, coined as exosome-mimetic nanovesicles (NV), to combine the characteristics of cells and nanocarriers and applied to targeted delivery of anticancer chemotherapeutics. By subjecting cells of different origin to serial extrusion through filters with diminishing pore sizes after the cells had been loaded with chemotherapeutic agents, we generated high quantities of exosome-mimetic NV carrying sheltered drugs. Using this system, we investigated whether the

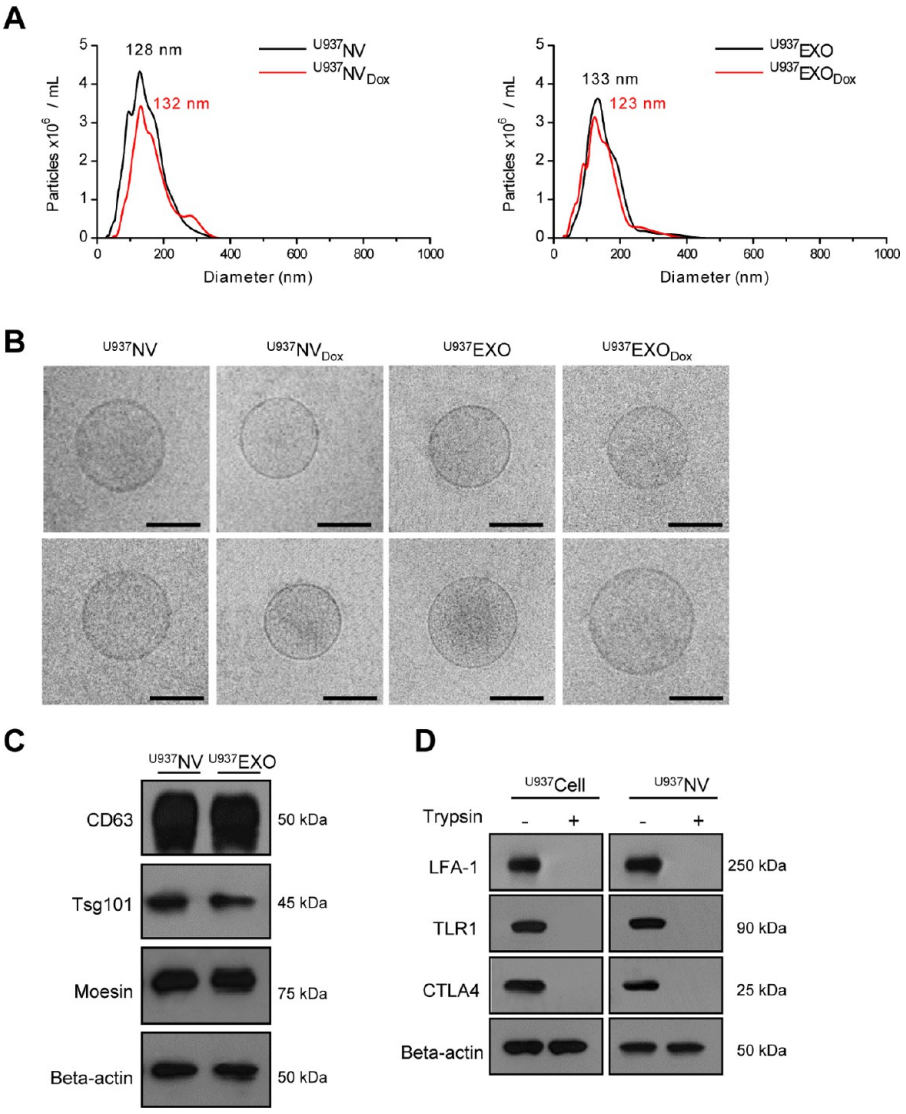


**Figure 2. Characterization of NV and doxorubicin-loaded NV. (A) Size distribution of $^{U937}$NV, $^{U937}$NV$_{Dox}$, $^{U937}$EXO, and $^{U937}$EXO$_{Dox}$ measured by nanoparticle tracking analysis. (B) Representative cryotransmission electron micrograph of $^{U937}$NV, $^{U937}$NV$_{Dox}$, $^{U937}$EXO, and $^{U937}$EXO$_{Dox}$. Scale bars: 100 nm. (C) Western blot analysis of exosomal marker proteins on $^{U937}$NV and $^{U937}$EXO (20 $\mu$g of total protein). (D) Topology of plasma membrane proteins in the $^{U937}$NV. After $^{U937}$Cell and $^{U937}$NV were incubated with trypsin, each sample (20 $\mu$g of total protein) was analyzed by Western blotting using anti-LFA-1, Toll-like receptor (TLR) 1, and CTLA-4 antibodies. Dox: doxorubicin; EXO: exosomes.**

chemotherapeutic drugs were delivered more efficiently when compared with the free drug alone, drug-loaded nanosized exosomes, or drug-loaded microsized cells using *in vitro* human endothelial cell model and *in vivo* mouse tumor model.

## RESULTS AND DISCUSSION

**Production and Characterization of Exosome-Mimetic NV.** To obtain a pool of cell-derived NV and doxorubicin-loaded NV, human U937 monocytic cells were harvested and serially extruded through a series of polycarbonate membranes with pore sizes of 10, 5, and finally 1 $\mu$m in the absence or presence of various concentrations of doxorubicin (Figure 1A). These vesicles were termed $^{U937}$NV and $^{U937}$NV$_{Dox}$, respectively. We purified $^{U937}$NV and $^{U937}$NV$_{Dox}$ from the interface between the 10 and 50% iodixanol layers in a two-step OptiPrep density gradient ultracentrifugation. Doxorubicin packaging into $^{U937}$NV$_{Dox}$ was dependent on the drug concentration in the cell suspension solution: 52.1 $\pm$ 5.3 ng, 214.5 $\pm$ 34.9 ng, or 332.4 $\pm$ 44.2 ng of doxorubicin was associated with 1 $\mu$g of $^{U937}$NV$_{Dox}$ (measured on the basis of total protein concentration) when 100, 200, or 400 $\mu$g/mL of doxorubicin was used, respectively (Figure 1B). In this study, we used $^{U937}$NV$_{Dox}$ that were prepared by using 400 $\mu$g/mL of doxorubicin. Using 1 $\times$ $10^7$ U937 cells, we obtained 203 $\mu$g of total protein and 210 $\times$ $10^9$ particles of $^{U937}$NV (Figure 1C,D). However, we observed that the same number of cells cultured for 24 h produced only 1.74 $\mu$g of total protein and 2.00 $\times$ $10^9$ particles of exosomes ($^{U937}$EXO). Thus, by deriving exosome-mimetic

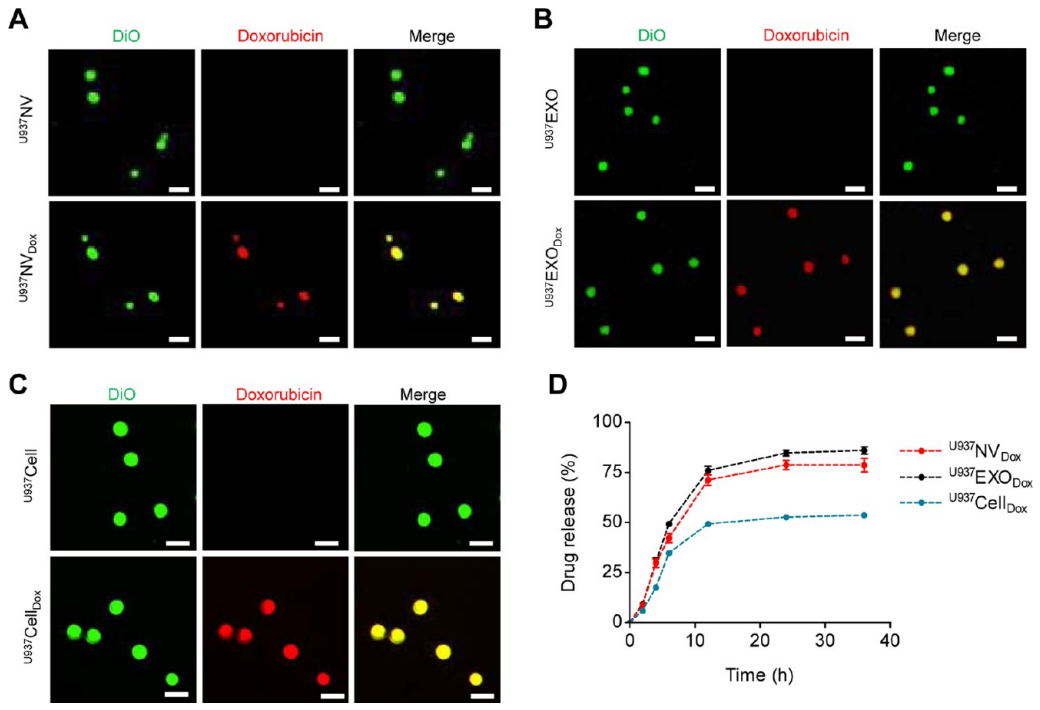


**Figure 3. Identification of doxorubicin on NV, exosomes, and cells. (A−C) Representative fluorescence microscopy images of $^{U937}$NV and $^{U937}$NV$_{Dox}$ (A), $^{U937}$EXO and $^{U937}$EXO$_{Dox}$ (B), and $^{U937}$Cell and $^{U937}$Cell$_{Dox}$ (C), labeled with DiO membrane dye. DiO and doxorubicin are shown as green fluorescent signals and red fluorescent signals, respectively. The merged signals for DiO and doxorubicin are indicated by yellow fluorescence. Scale bars: 1 $\mu$m for (A) and (B), 20 $\mu$m for (C). (D) Kinetics of doxorubicin release from $^{U937}$NV$_{Dox}$, $^{U937}$EXO$_{Dox}$, and $^{U937}$Cell$_{Dox}$ as determined by incubation for up to 36 h in PBS ($n$ = 3). Data are presented as the mean ± SD. Dox: doxorubicin; EXO: exosomes.**

NV through homogenization of cultured U937 cells, we increased the yield of total protein and particle number more than 100-fold higher than that of naturally produced exosomes.

Nanoparticle tracking analysis of the purified $^{U937}$NV and $^{U937}$NV$_{Dox}$ showed a size distribution with a peak diameter of approximately 120−130 nm similar to those of $^{U937}$EXO and $^{U937}$EXO$_{Dox}$ (Figure 2A). Examination of the purified NV and exosomes using cryo-TEM revealed that they were closed vesicles devoid of the parent cells, cellular debris, and protein aggregates (Figure 2B). In addition, the purified $^{U937}$NV contained exosomal marker proteins including CD63, Tsg101, moesin, and beta-actin (Figure 2C).[29] All these results suggest that cell-derived NV have similarity with exosomes in size, morphology, and protein contents. Treatment of the intact $^{U937}$NV with trypsin eliminated extracellular domains of plasma membrane proteins (LFA-1, Toll-like receptor 1, and CTLA-4) in the NV, which shows that the NV has the same topology as the parent cells (Figure 2D). Additionally, NV or doxorubicin-loaded NV were reproducibly generated from adherent cells such as the Raw264.7 (immortalized mouse macrophages; Figure S1, Supporting Information).

The introduction of doxorubicin into the NV, exosomes, and cells was determined by fluorescence microscopy, as doxorubicin is autofluorescent.[30] When NV, exosomes, and cells were labeled with DiO green fluorescent membrane dye, only $^{U937}$NV$_{Dox}$, $^{U937}$EXO$_{Dox}$, and $^{U937}$Cell$_{Dox}$ were double-positive for both the red fluorescence of doxorubicin and the green fluorescence of DiO (Figure 3A,B,C). This result shows that the doxorubicin is associated with the $^{U937}$NV$_{Dox}$, $^{U937}$EXO$_{Dox}$, and $^{U937}$Cell$_{Dox}$. Furthermore, we determined the efflux of doxorubicin from the $^{U937}$NV$_{Dox}$, $^{U937}$EXO$_{Dox}$, and $^{U937}$Cell$_{Dox}$ after the incubation up to 36 h in phosphate-buffered saline (PBS): 42.2 ± 3.9%, 49.2 ± 2.1%, and 34.7 ± 1.9% of the doxorubicin was released within 6 h, and doxorubicin release was saturated at 78.6 ± 5.7%, 85.9 ± 3.1%, and 53.6 ± 1.7% at 36 h, respectively (Figure 3D).

***In Vitro* Targeted Delivery of Chemotherapeutic Drugs Using NV.** Extravasation of leukocytes including monocytes into the inflamed tissues is vital for immune surveillance and inflammation.[31] The interaction between cell adhesion molecules (CAMs, for example, ICAM-1, VCAM-1, and E-selectin) overexpressed on the inflamed endothelium and counter-receptors for endothelial CAMs (for example, LFA-1) on the circulating leukocytes plays critical role in these leukocyte recruitment processes.[31,32] It is well-known that inflammatory cytokines including TNF-α induce the cell surface expression of CAMs in vascular endothelial cells.[33] As reported, human umbilical vein endothelial cells (HUVECs) treated with TNF-α demonstrate significantly increased expression of ICAM-1, VCAM-1, and E-selectin, which significantly increase the adhesion of human U937 monocytic cells or mouse Raw264.7 macrophages to HUVECs (data not shown). We previously

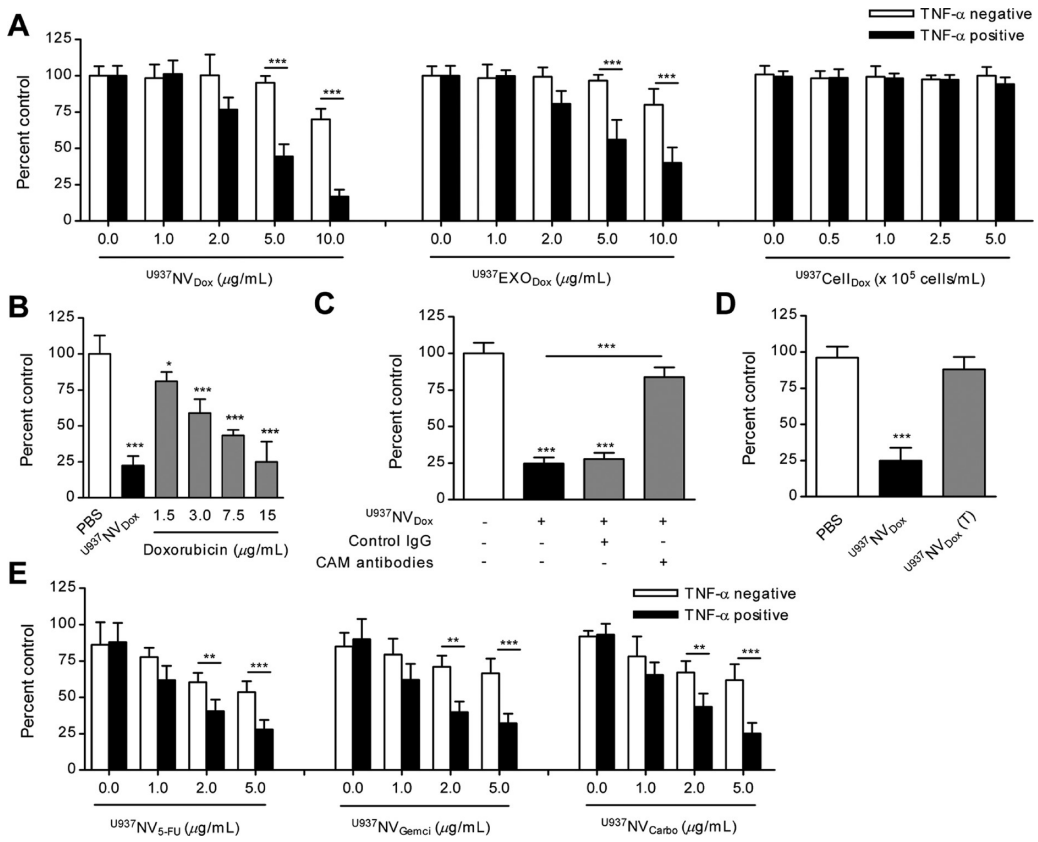


**Figure 4.** ***In vitro*** **targeted delivery of chemotherapeutics using NV. (A) Concentration-dependent cytotoxic effect of $^{U937}NV_{Dox}$, $^{U937}EXO_{Dox}$, and $^{U937}Cell_{Dox}$ on TNF-α treated and untreated HUVECs ($n$ = 6/group). (B) Comparison of the cytotoxic effect of $^{U937}NV_{Dox}$ (5 μg/mL of total protein) with that of varying doses of free doxorubicin on TNF-α-treated HUVECs ($n$ = 6/group). Note that 1.5 μg of doxorubicin is loaded into the $^{U937}NV_{Dox}$ (5 μg of total protein). (C) Preincubation with a neutralizing antibody cocktail against ICAM-1 (10 μg/mL), VCAM-1 (30 μg/mL), and E-selectin (50 μg/mL) blocked the cytotoxic effect of $^{U937}NV_{Dox}$ (5 μg/mL of total protein) on TNF-α-treated HUVECs ($n$ = 6/group). (D) Effect of trypsin-treated $^{U937}NV_{Dox}$ on TNF-α-treated HUVECs ($n$ = 5/group). All samples were treated with 5 μg/mL of total protein. (E) Concentration-dependent cytotoxic effect of $^{U937}NV_{5\text{-}FU}$, $^{U937}NV_{Gemci}$, and $^{U937}NV_{Carbo}$ on TNF-α-treated and untreated HUVECs ($n$ = 6/group). Data are presented as the mean ± SD *$P$ < 0.05, **$P$ < 0.01, *** $P$ < 0.001. EXO: exosomes; Dox: doxorubicin; Gemci: gemcitabine; Carbo: carboplatin.**

showed that $^{U937}NV$ (produced from the human U937 monocytic cells) harbor the counter-receptor(s) for endothelial CAM(s), for example, LFA-1, on their surface (Figure 2D). Therefore, we can speculate that $^{U937}NV_{Dox}$ mediate targeted delivery of chemotherapeutic drugs to TNF-α-treated endothelial cells expressing ICAM-1, VCAM-1, and E-selectin on their cell surface. As expected, treatment of $^{U937}NV_{Dox}$ induced cell death more efficiently in TNF-α-treated HUVECs compared to untreated HUVECs (Figure 4A). However, $^{U937}NV$ without doxorubicin (up to 50 μg/mL of total protein) did not induce cell death in TNF-α-treated or untreated HUVECs (Figure S2, Supporting Information). When compared with $^{U937}NV_{Dox}$, $^{U937}EXO_{Dox}$ resulted in similar cell death rates in TNF-α-treated HUVECs while $^{U937}Cell_{Dox}$ did not (Figure 4A). This result suggests that nanosized $^{U937}NV_{Dox}$ or $^{U937}EXO_{Dox}$ are more cytotoxic on TNF-α-treated HUVECs than microsized $^{U937}Cell_{Dox}$. Moreover, $^{U937}NV_{Dox}$ (5 μg/mL containing 1.5 μg/mL of doxorubicin) resulted in cytotoxicity similar to that observed for 15 μg/mL of free doxorubicin (Figure 4B), which suggests that $^{U937}NV_{Dox}$ have a delivery efficiency that is approximately 10-fold higher than that of free doxorubicin. Additionally, $^{Raw264.7}NV_{Dox}$ (produced from the mouse Raw264.7 macrophages) had a cytotoxic effect in TNF-α-treated HUVECs that was similar to that of $^{U937}NV_{Dox}$ originated from human U937 cells (Figure S3, Supporting Information).

The addition of a cocktail of neutralizing antibodies against ICAM-1, VCAM-1, and E-selectin effectively reduced $^{U937}NV_{Dox}$-induced cytotoxicity in TNF-α-treated HUVECs (Figure 4C). Application of trypsin to $^{U937}NV_{Dox,}$ (which removes the extracellular domains of counter-receptors for endothelial CAMs including LFA-1 on NV), abolished the effect of the $^{U937}NV_{Dox}$ (Figure 4D). This finding suggests that the presence of counter-receptors for endothelial CAMs on the surface of $^{U937}NV_{Dox}$ is important for targeted delivery of doxorubicin to TNF-α-treated endothelial cells, which express ICAM-1, VCAM-1, and E-selectin on their cell surface.

Furthermore, NV loaded with other anticancer chemotherapeutics were developed using 400 μg/mL of 5-FU, gemcitabine (Gemci), or carboplatin (Carbo). All

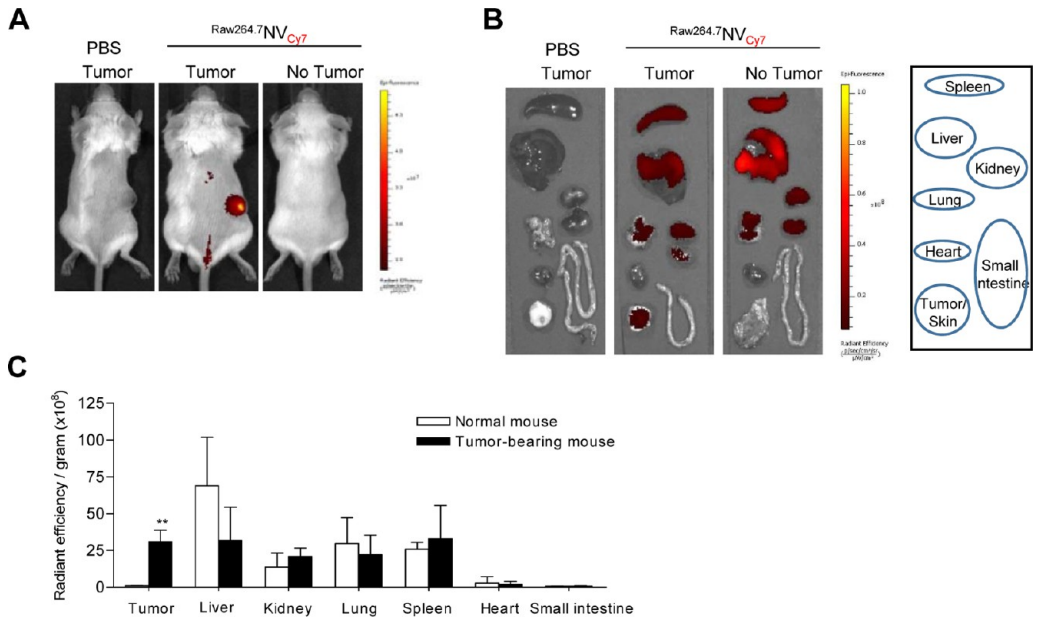


**Figure 5.** ***In vivo*** **targeting of Cy7-labeled $^{Raw264.7}$NV to tumors in mice. (A−C) CT26 cells (mouse colon adenocarcinoma; $1 \times 10^6$ cells) were injected subcutaneously into BALB/c mice. Fourteen days later, the mice were treated by intravenous injections of Cy7-labeled $^{Raw264.7}$NV (50 $\mu$g of total protein) or PBS. Normal mice without tumors were used as the control. After 12 h, the Cy7 fluorescence of the whole mouse body (A) or various tissues (B) was acquired by IVIS spectrum. Radiant efficiency was measured using Living Image 3.1 software and normalized to tissue weight (C; $n$ = 4/group). Data are presented as the mean ± SEM ** $P < 0.01$.**

of these chemotherapeutics-loaded $^{U937}$NV also induced cell death in a concentration-dependent manner, with higher potency in TNF-α-treated HUVECs (Figure 4E). Together, these results demonstrated that NV can harbor various chemotherapeutics and deliver them to the target cells.

***In Vivo*** **Targeting of NV to Tumors in Mice.** We assessed the targeting ability of $^{Raw264.7}$NV (produced from the mouse Raw264.7 macrophages) to the tumor tissue *in vivo* using BALB/c mice bearing subcutaneously transplanted CT26 cells. Cy7 labeled-$^{Raw264.7}$NV were injected intravenously into CT26-tumor-bearing mice. Whole-mouse imaging showed strong accumulation of Cy7 fluorescence in the tumor area for intact $^{Raw264.7}$NV (Figure 5A). The distribution of Cy7 fluorescence in different organs in animals with and without tumors is shown in Figure 5B,C. Strong accumulation of Cy7 fluorescence was observed in tumors, but not in the corresponding skin areas in mice without tumors. Cy7 fluorescence was also observed in the spleen, liver, kidney, and lung after $^{Raw264.7}$NV$_{Cy7}$ injection, but not in the heart, which is an organ sensitive to doxorubicin.[34]

It is known that tumor endothelium expresses CAMs such as ICAM-1 in a significantly higher degree than healthy tissue endothelium.[35,36] As reported, we observed that ICAM-1 was expressed in the transplanted CT26 tumor endothelium, but not in the skin, liver, heart, and kidney (Figure S4, Supporting Information). All these organs including tumor did not express VCAM-1 and E-selectin (data not shown). The distribution of autofluorescent doxorubicin administered in $^{Raw264.7}$NV$_{Dox}$ or as a free drug is shown for different organs in Figure 6. Importantly, the fluorescence of doxorubicin administered in $^{Raw264.7}$NV$_{Dox}$ was significantly increased in tumors, primarily in the endothelium, but not in the skin and heart: doxorubicin accumulated primarily in the nonendothelial parenchyma of the liver and kidney. By contrast, doxorubicin administered as a free drug appeared in the heart, liver, and kidney but did not accumulate in the tumor tissue. In addition, trypsinization of the $^{Raw264.7}$NV$_{Dox}$, which removed the extracellular domains of plasma membrane proteins including LFA-1 on NV (Figure 2D), significantly reduced the accumulation of doxorubicin in tumors. All these findings suggest that exosome-mimetic nanovesicles work well for targeted delivery of chemotherapeutics to malignant tumors.

**Inhibition of Primary Tumor Growth by $^{Raw264.7}$NV$_{Dox}$ in a Mouse Syngeneic Model.** To determine the antitumor activity of $^{Raw264.7}$NV$_{Dox}$ (produced from the mouse Raw264.7 macrophages), we utilized a model of mouse CT26 colorectal cancer cell line introduced subcutaneously to immunocompetent BALB/c mice. Five days after the introduction of the CT26 tumor cells, treatment with intravenous injection of $^{Raw264.7}$NV$_{Dox}$ (10 $\mu$g of total protein) was commenced and resulted in significant attenuation of tumor growth (Figure 7A,B). In contrast, $^{Raw264.7}$NV that did not contain doxorubicin (10 $\mu$g of total protein) did not affect tumor growth (Figure 7A,B). Neither a loss in body weight (Figure 7C) nor a decrease in white blood cell count (Figure 7D) was observed following $^{Raw264.7}$NV$_{Dox}$ or $^{Raw264.7}$NV

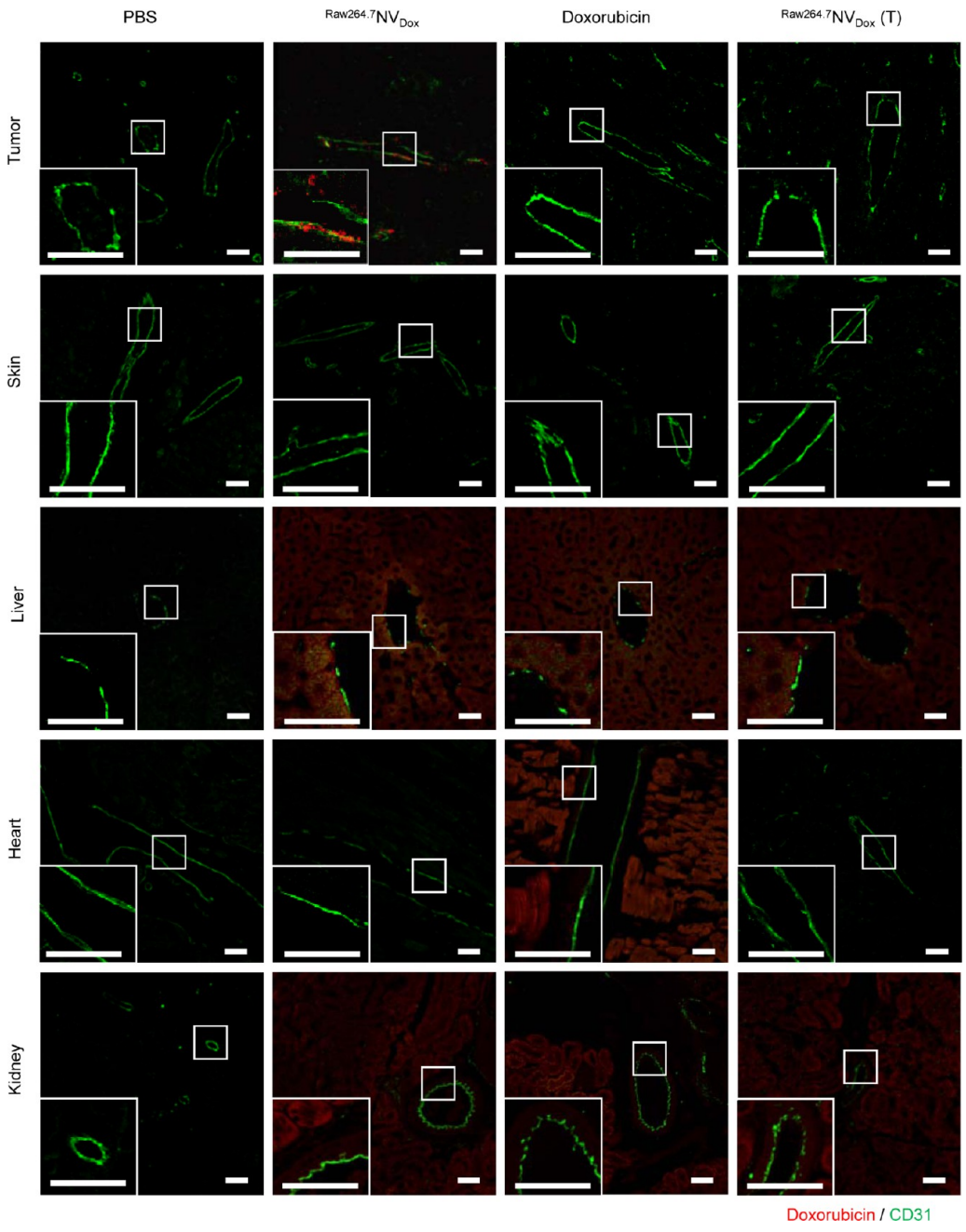


**Figure 6.** *In vivo* **doxorubicin distribution after $^{Raw264.7}NV_{Dox}$ injection. One million CT26 cells were injected subcutaneously into BALB/c mice. Fourteen days later, the mice were treated by intravenous injections of $^{Raw264.7}NV_{Dox}$ (100 $\mu$g of total protein), trypsin-treated $^{Raw264.7}NV_{Dox}$ (100 $\mu$g of total protein), free doxorubicin (30 $\mu$g), or PBS. The mice were sacrificed and tissues were extracted. The extracted tissues were embedded in paraffin, sectioned, and analyzed by immunohistochemistry. Endothelium is identified by the green fluorescence signal of CD31, and doxorubicin is identified by the red fluorescence signal. Note that 30 $\mu$g of doxorubicin was loaded into $^{Raw264.7}NV_{Dox}$ (100 $\mu$g of total protein). $^{Raw264.7}NV_{Dox}$ (T): trypsin-treated $^{Raw264.7}NV_{Dox}$. Scale bars, 30 $\mu$m.**

treatment. The density of cells in the tumor that were positive for the endothelial cell marker CD31 was dose-dependently reduced by the $^{Raw264.7}NV_{Dox}$ (Figure 7E). The TUNEL and phosphohistone 3 staining of serially sectioned tumor tissues showed that the $^{Raw264.7}NV_{Dox}$ dose-dependently increased apoptosis in cells in the vicinity of the tumor endothelium (Figure 7F) and reduced the number of proliferating cells in the tumor when compared with tissues in control mice (Figure 7G,H). However, $^{Raw264.7}NV_{Dox}$ showed no *in vitro* cytotoxic effect on CT26 cells (Figure S5, Supporting Information), which do not express ICAM-1, VCAM-1, or E-selectin.[36] Angiogenesis, the formation and growth of new blood vessels from the pre-existing vasculature, is critical for tumor growth.[37−39] Although antiangiogenesis therapy does not guarantee complete tumor regression, it is considered a promising antitumor therapy.[37,38] Taken together, our results suggest that $^{Raw264.7}NV_{Dox}$ exhibit

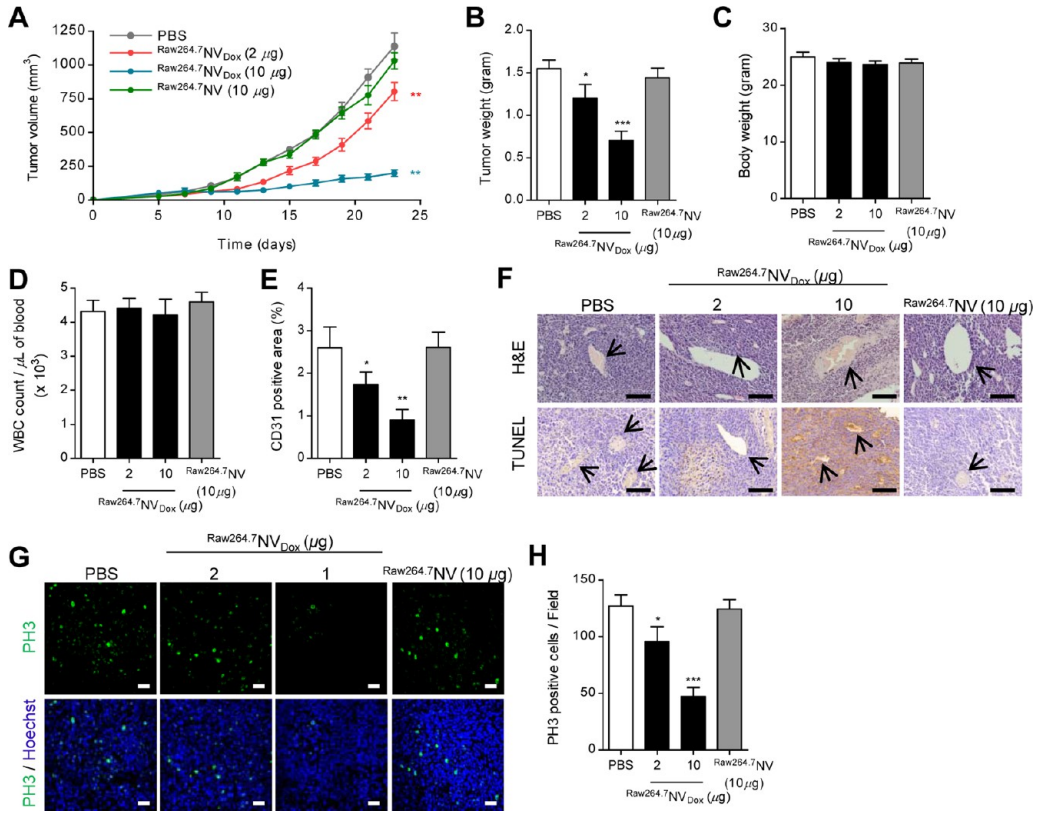


**Figure 7. Antitumor effects of doxorubicin-loaded NV in a mouse syngeneic model. (A−H) Antitumor effect induced by $^{Raw264.7}NV_{Dox}$ ($n$ = 10/group). Tumor volume was determined every second day (A), and tumor tissues were extracted and weighed (B) at the end of experiments. Panels (C) and (D) show body weight and white blood cells (WBC) at the end of the experiment, respectively. (E) The calculated CD31-positive area of the confocal microscopy images of tumor tissues stained with CD31 (endothelium; $n$ = 10/group). (F) H&E- and TUNEL-stained tumor tissues (arrows indicate endothelium). (G) Representative confocal microscopy images of tumor tissues stained with phosphohistone 3 (PH3, green) and Hoechst (blue). (H) The calculated number of PH3-positive cells ($n$ = 10/group). Scale bars: 200 $\mu$m for (F) and 30 $\mu$m for (G). Data are presented as the mean ± SEM * $P$ < 0.05, ** $P$ < 0.01, *** $P$ < 0.001. All $P$-values shown are *vs* PBS control. Dox: doxorubicin.**

the antitumor activity *in vivo* indirectly, through an antiangiogenesis effect. However, we could not exclude the possibility that $^{Raw264.7}NV_{Dox}$ adherent to the tumor endothelium could continuously release doxorubicin in the tumor microenvironment. The detailed mechanisms of antitumor activity caused by $^{Raw264.7}NV_{Dox}$ *in vivo* require further elucidation.

**Comparison of Antitumor Effects of $^{Raw264.7}NV_{Dox}$ with Free Doxorubicin, Doxorubicin-Loaded Exosomes, Liposomal Doxorubicin, Trypsin-Treated $^{Raw264.7}NV_{Dox}$, and Doxorubicin-Loaded Cells in a Mouse Syngeneic Model.** We next compared the therapeutic index of $^{Raw264.7}NV_{Dox}$ with free doxorubicin, by comparing antitumor effects and effects on the number of circulating white blood cells. Free doxorubicin (3 $\mu$g) at a dose equivalent to that of doxorubicin loaded in 10 $\mu$g of the total protein of the $^{Raw264.7}NV_{Dox}$ had no significant effect on tumor growth (Figure 8A,B). Treatment with doxorubicin at a dose of 60 $\mu$g resulted in an antitumor effect similar to that of $^{Raw264.7}NV_{Dox}$ (10 $\mu$g of total protein), but reduced both white blood cell counts (Figure 8C) and body weight (Figure 8D) compared with the $^{Raw264.7}NV_{Dox}$. Moreover, although the injection of $^{Raw264.7}NV_{Dox}$ or doxorubicin resulted in the accumulation of doxorubicin in the liver (Figure 6), any hepatic toxicity was not observed following $^{Raw264.7}NV_{Dox}$ (10 $\mu$g of total protein) or doxorubicin (60 $\mu$g) treatment (Table S1, Supporting Information). However, the hepatic injury was observed after 24 h intravenous administration of $CCl_4$ (40% in corn oil), which is a well-known liver toxic agent.[40] These results thus argue that doxorubicin administered by the NV can significantly improve its therapeutic index.

Using immunocompetent BALB/c mice bearing CT26 tumors, we further compared the antitumor activity of doxorubicin-loaded NV and exosomes. In this study, we used exosomes derived from the human U937 monocytic cells because mouse Raw264.7 macrophages release relatively low quantities of exosomes. Studies show that human monocytic cells can adhere to the mouse endothelium by the interaction between mouse endothelial CAMs and their counter-receptors on the human monocytes.[41−45] Treatment of the mice with $^{U937}NV_{Dox}$ resulted in antitumor effects similar to the effects observed with $^{U937}EXO_{Dox}$ and $^{Raw264.7}NV_{Dox}$ (produced from the mouse Raw264.7 macrophages) on tumor volume (Figure 8E) and tumor weight at the end of the experiments (Figure S6A, Supporting Information), whereas injections with the $^{U937}EXO$,

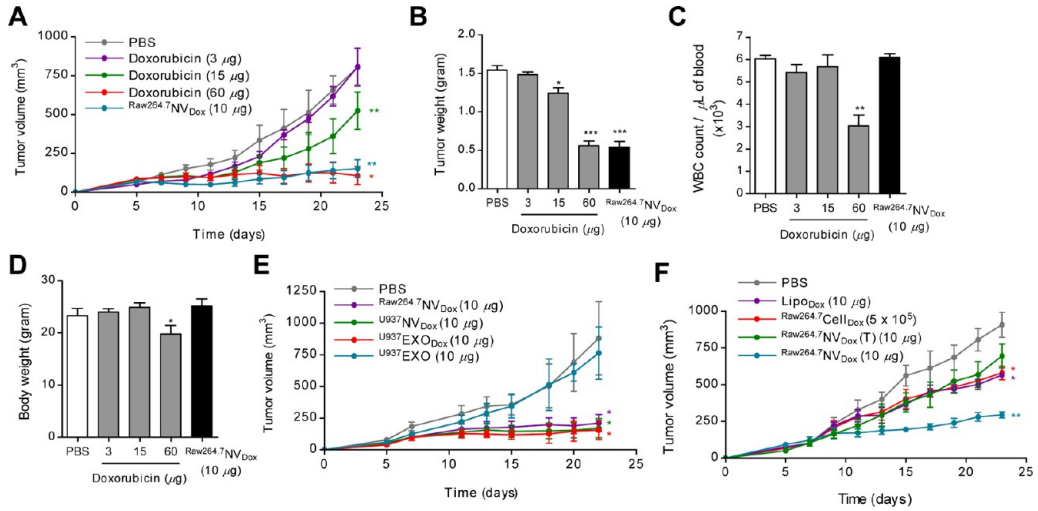


**Figure 8. Comparison of antitumor effects of $^{Raw264.7}NV_{Dox}$ with free doxorubicin, doxorubicin-loaded exosomes, liposomal doxorubicin, trypsin-treated $^{Raw264.7}NV_{Dox}$, and doxorubicin-loaded cells in a mouse syngeneic model. (A–D) Comparison of the antitumor activity of $^{Raw264.7}NV_{Dox}$ with that of varying doses of free doxorubicin ($n$ = 5/group), and panels (C) and (D) show white blood cells (WBC) and body weight at the end of the experiment, respectively. Note that 3 $\mu$g of doxorubicin is loaded in $^{Raw264.7}NV_{Dox}$ (10 $\mu$g of total protein). See also Table S1 (Supporting Information) for hepatic injury analysis. (E) Comparison of the antitumor activity of $^{U937}NV_{Dox}$ with that of $^{U937}EXO_{Dox}$ ($n$ = 5/group). (F) Comparison of the antitumor activity of $^{Raw264.7}NV_{Dox}$ (10 $\mu$g of total protein) with that of $^{Raw264.7}Cell_{Dox}$, liposomal doxorubicin, and $^{Raw264.7}NV_{Dox}$ (T) ($n$ = 5/group). Each injected treatment harbored 3 $\mu$g of doxorubicin. Data are presented as the mean ± SEM * $P$ < 0.05, ** $P$ < 0.01, *** $P$ < 0.001. All $P$-values shown are *vs* PBS control. Dox: doxorubicin; EXO: exosomes.**

which are not loaded with doxorubicin, had no significant effects. These data show that the effects of doxorubicin-loaded NV and exosomes treatment are similar, suggesting (1) that the NV mimic the targeting capacity of the exosomes, and (2) that NV can be used as an alternative of exosomes as drug delivery systems. This is important, since the yield of NV is approximately 100-fold higher than exosomes (Figure 1C,D). We further compared the *in vivo* antitumor effects of $^{Raw264.7}NV_{Dox}$ with doxorubicin-loaded whole Raw264.7 cells ($^{Raw264.7}Cell_{Dox}$), liposomal doxorubicin ($Lipo_{Dox}$), and trypsin-treated $^{Raw264.7}NV_{Dox}$. The $^{Raw264.7}Cell_{Dox}$, $Lipo_{Dox}$, and $^{Raw264.7}NV_{Dox}$ (T) showed decreased antitumor effects when compared with the $^{Raw264.7}NV_{Dox}$ (Figure 8F and Figure S6B, Supporting Information), despite the use of the same dose of doxorubicin in all cases. This result suggests that (1) the antitumor effect of nanosized $NV_{Dox}$ was significantly greater than microsized $Cell_{Dox}$, and (2) the presence of the membrane proteins on the surface of the $^{Raw264.7}NV_{Dox}$ is important for targeted delivery of doxorubicin to malignant tumors.

## CONCLUSIONS

In this paper, we report a series of experiments to describe the production and therapeutic effect of bioinspired exosome-mimetic nanovesicles that were loaded with chemotherapeutic drugs. The exosome-mimetic nanovesicles loaded with doxorubicin reduced tumor growth to the same extent as 20-fold higher doses of free drug but without systemic side effects.

We developed exosome-mimetic nanovesicles that target endothelial cells by producing the nanovesicles from cells that harbor the counter-receptors for endothelial CAMs, for example, LFA-1. Tumors demonstrate abnormal angiogenesis, with rapidly proliferating endothelial cells that express CAMs and support tumor growth.[46] Chemotherapeutic-loaded nanovesicles generated from macrophages and monocytes effectively bind to endothelial cells, which result in delivery of the chemotherapeutics and subsequent cell death. Importantly, removal of the ligands to the endothelial CAMs by trypsinization eliminated the therapeutic effects of the nanovesicles both *in vitro* and *in vivo*. Liposomes developed from pure lipids that did not harbor targeting proteins were inefficient in reducing tumor growth in our models, even though they were loaded with the same amount of the drug. Whole cells that contained the same surface molecules as the exosome-mimetic nanovesicles were also inefficient in treating tumors *in vivo*, which suggests that the nano size of exosome-mimetic nanovesicles is crucial to achieve effective targeted delivery.

Exosomes harvested from the same cells that were used to produce exosome-mimetic nanovesicles were similarly effective in treating tumors *in vivo*, as has been found previously using a stat-3 inhibitor.[23] These results suggest that membrane-derived nanovesicles are efficient for the targeted delivery of chemotherapeutics, regardless of whether they are produced naturally or artificially from cells. However, the yield of exosome-mimetic nanovesicles was more than 100-fold higher than that of exosomes from the same number of cells. To improve the antitumor activity of exosome-mimetic nanovesicles, future treatments may utilize the combinations of nanovesicles containing different targeting molecules, which may thus home

to both the endothelium and the tumor cells.[47] Furthermore, this technology could prove beneficial for the delivery of siRNA with improved yield, as siRNA-loaded exosomes were found to be efficient in a previous report.[25] Exosome-mimetic nanovesicles could also be used for theragnosis by loading with *in vivo* imaging molecules and chemotherapeutics.[48,49] Lastly, different types of cells could be engineered to express specific targeting molecules to enhance therapeutic antitumor efficacy. However, the overall safety, systemic immune response, and efficacy of exosome-mimetic nanovesicles versus exosomes require further elucidation.

In conclusion, this report demonstrates a proof of concept for the efficient treatment of tumors using chemotherapeutics-loaded exosome-biomimicry, but only when the source cells used express the appropriate targeting molecules on their surfaces, either naturally or through genetic engineering.

## METHODS

**Cell Culture.** Human umbilical vein endothelial cells (HUVECs) were isolated from human umbilical cord veins and cultured as described previously.[50] The cells were grown in M199 medium containing bFGF (3 ng/mL) and heparin (5 units/mL), and they were used at passage six in all experiments. U937 cells, Raw264.7 cells, and CT26 cells were grown in RPMI 1640 medium, Dulbecco's Modified Eagle Medium, and Minimum Essential Medium, respectively. All media were supplemented with 10% FBS and 1% Antibiotic-Antimycotic (Invitrogen). All cells not contaminated by mycoplasma were cultured at 37 °C in a humidified atmosphere of 5% $CO_2$. Cell culture reagents were purchased from Gibco-BRL.

**Animals.** All experiments using animal models were approved by the Institutional Animal Care and Use Committee at POSTECH, Pohang, Republic of Korea (approval number: 2011-01-0020). BALB/c was purchased from Jackson Laboratories. The mice were bred in the pathogen-free facility at POSTECH.

**Preparation of Nanovesicles (NV) and Chemotherapeutics-Loaded NV.** Cells were resuspended at a concentration of $5 \times 10^6$ cells/mL in phosphate-buffered saline (PBS) with or without chemotherapeutics. Adherent cells were detached by scraping. The cell suspension was sequentially extruded three times through 10, 5, and 1 $\mu$m polycarbonate membrane filters (Whatman) using a mini-extruder (Avanti Polar Lipids). To form a step gradient, 50% iodixanol (Axis-Shield PoC AS) was placed at the bottom of an ultracentrifuge tube, overlaid with 10% iodixanol and the extruded samples, and then ultracentrifuged at 100000*g* for 2 h at 4 °C. NV and chemotherapeutics-loaded NV were obtained from the interface of the 50 and 10% iodixanol layers.

**Preparation of Exosomes and Doxorubicin-Loaded Exosomes.** Exosome-depleted FBS was prepared by ultracentrifugation at 150000*g* for 16 h at 4 °C.[51] Exosomes were isolated as previously described with modifications.[39] U937 cells were incubated in RPMI medium containing 10% exosome-depleted FBS for 24 h. Cells and debris were eliminated by serial centrifugation at 500*g* for 10 min and 3000*g* for 15 min at 4 °C. Exosomes were pelleted by ultracentrifugation at 150000*g* for 2 h at 4 °C and resuspended in PBS. Protein was quantified using the Bradford assay and adjusted to a concentration of 1 mg/mL with PBS. Half of the isolated exosomes were incubated with 400 $\mu$g/mL of doxorubicin for 2 h at 37 °C. A two-step OptiPrep density gradient ultracentrifugation was performed as described above. Exosomes and doxorubicin-loaded exosomes were obtained from the interface of the 50 and 10% OptiPrep layers.

**Preparation of Doxorubicin-Loaded Cells.** U937 or Raw264.7 cells were resuspended at a concentration of $5 \times 10^6$ cells/mL in PBS, and incubated with 400 $\mu$g/mL of doxorubicin for 2 h at 37 °C. Doxorubicin-loaded cells were harvested by centrifugation at 500*g* for 10 min at 4 °C.

**Preparation of Doxorubicin-Loaded Liposomes.** Liposomal doxorubicin was prepared as previously described, with some modifications.[52] All lipids were purchased from Avanti Polar Lipids. *N*-(Carbonyl-methoxypolyethylene glycol 2000)-1,2-distearoyl-sn-glycero3-phosphoethanolamine sodium salt (MPEG-DSPE, 3.19 mg/mL), fully hydrogenated soy phosphatidylcholine (HSPC, 9.58 mg/mL), and cholesterol (3.19 mg/mL) were dissolved in chloroform, mixed, and evaporated under a vacuum. The lipid film was sonicated with ammonium sulfate (500 mM, pH 5.5) for 1 h at 56 °C using a 40-kHz Branson 2510 bath sonifier. Liposomes were subsequently extruded through polycarbonate membrane filters with a pore size of 100 nm. External ammonium sulfate was removed by dialysis against PBS. Doxorubicin (200 $\mu$g/mL) was added to the liposome preparation and incubated for 2 h at 37 °C. Free doxorubicin was removed by dialysis against PBS.

**Characterization of NV, Exosomes, and Cells.** To quantify the doxorubicin, 100 $\mu$L of doxorubicin-loaded NV, exosomes, and cells (30 $\mu$g/mL of total protein) were placed into the wells of 96-well plates. Doxorubicin fluorescence was detected using a Wallac 1420 VICTOR plate reader (Perkin-Elmer Life Sciences) with excitation/emission at 488 nm/530 nm.[53] The quantity of doxorubicin was calculated using a standard curve of free doxorubicin. For the doxorubicin release kinetics, $^{U937}NV_{Dox}$, $^{U937}EXO_{Dox}$, or $^{U937}Cell_{Dox}$ (40 $\mu$g of total protein) were suspended in 0.1 mL of PBS, loaded into Slide-A-Lyzer MINI dialysis units (molecular mass cutoff 10 kDa, Pierce), and dialyzed against 1 mL of PBS at 37 °C. The supernatant was harvested at 0, 3, 6, 12, 24, and 36 h. The doxorubicin released was quantified by fluorescence as described above.

Cryotransmission electron microscope images were obtained using a BIO-TEM installed at the Korea Basic Science Institute. The purified NV and exosomes (4 $\mu$L containing 500 $\mu$g/mL of total protein) were applied to a glow-discharged Quantifoil holey carbon grid (Spi Supplies) and subjected to plunge-freezing into liquid ethane with a FEI Vitrobot system (FEI). The frozen grids were then transferred to a FEI TECNAI G2 transmission electron microscope at liquid nitrogen temperature. Images were recorded at a magnification of 15 000−21 000 under low-dose (~50 e/Å$^2$) and 1−5 $\mu$m underfocus conditions using a Gatan 4000 by 4000 CCD camera (Gatan).

The size and particle number of NV and exosomes were assessed by nanoparticle tracking analysis using the Nanosight LM10-HS system (NanoSight). NV and exosomes (500 ng/mL of total protein) were dispersed in PBS and measured with camera level 9 and a 405-nm wavelength laser. The chamber temperature was 25 °C and maintained automatically. Measurements were obtained in triplicate, and each individual measurement duration was 1 min. Data were analyzed using nanoparticle tracking analysis software version 2.3 with a detection threshold of 5 (multiple), an autosetting of blur, a minimum track length of 10, and an autosetting for the minimum expected particle size.

To identify the colocalization of NV, exosomes, and cells with doxorubicin, 50 $\mu$L of each sample (20 $\mu$g/mL of total protein) was labeled with DiO (1 $\mu$M, Invitrogen) fluorescent dye and incubated overnight on a cover glass at 4 °C. Coated samples were analyzed using an Olympus IX81 microscope.

***In Vitro* Cytotoxicity of Cells.** All experiments were conducted in 10% FBS-containing medium. HUVECs ($3 \times 10^4$ cells) were plated onto a gelatin-coated cover glass and incubated for 16 h in the presence or absence of TNF-α (10 ng/mL, R&D systems). Chemotherapeutics-loaded NV or other appropriate samples were added for 20 min and then exchanged for fresh media. After 24 h, cells were washed once with PBS and incubated with 5 $\mu$M 5-chloromethylfluorescein diacetate (CMFDA, Molecular Probes) in serum-free M199 medium for 1 h. After washing with PBS, cells were fixed with 4% paraformaldehyde for 10 min and observed with an Olympus IX81 microscope, and live cells were counted. For treatment with neutralizing antibodies, TNF-α-treated

HUVECs were incubated with a cocktail of anti-ICAM-1 (10 $\mu$g/mL), anti-VCAM-1 (30 $\mu$g/mL), and anti-E-selectin (50 $\mu$g/mL) antibodies or normal mouse IgG (90 $\mu$g/mL) for 30 min and then incubated with $^{U937}NV_{Dox}$ (5 $\mu$g/mL of total protein) for 20 min. All antibodies were purchased from R&D Systems.

**Syngeneic CT26 Tumor Model and *in Vivo* Antitumor Effects.** Male BALB/c mice (5−6 weeks old) were engrafted subcutaneously with $1 \times 10^6$ CT26 mouse colon adenocarcinoma cells in the right flank. Tumor volume ($mm^3$) was calculated as $(\text{width})^2 \times (\text{length}) \times 0.5$, as described previously.[54] At day 5, the mice were randomly divided into several groups according to the experimental protocol. Each subject was injected intravenously every other day. At the end of the experiment (day 22 or 23), blood was harvested by heart puncture, and the white blood cells (WBCs) in the blood were counted after red blood cell lysis by treatment with 1% HCl for 10 min at room temperature. The tumor tissue was excised and weighed. Serum was obtained at the end of the experiment (day 23), and the hepatic injury markers were analyzed using the chemistry analyzer BS-290 (Mindray). As a positive control, the hepatic injury was observed after 24 h intravenous administration of $CCl_4$ (40% in corn oil).[40]

***In Vivo* Targeting in the CT26 Syngeneic Tumor Model.** $^{Raw264.7}NV$ were incubated with Cy7 monoNHS ester (5 $\mu$M, Amersham Biosciences) for 2 h at 37 °C. Cy7-labeled samples were isolated using the two-step OptiPrep density gradient ultracentrifugation method. Cy7-labeled $^{Raw264.7}NV$ (50 $\mu$g of total protein) were injected intravenously to CT26 tumor-bearing mice. After 12 h, Cy7 fluorescence in the whole body of the mice was acquired by IVIS spectrum (Caliper Life Sciences). Mice were sacrificed, and Cy7 fluorescence was quantified in tissues including the tumor, liver, heart, kidney, spleen, lung, and small intestine. Radiant efficiency was measured using Living Image 3.1 software and normalized by tissue weight.

To analyze the doxorubicin distribution in the mice, $^{Raw264.7}NV_{Dox}$ (100 $\mu$g of total protein), $^{Raw264.7}NV_{Dox}$ (T) (100 $\mu$g of total protein), free doxorubicin (30 $\mu$g), and PBS were injected intravenously into CT26-tumor-bearing mice. After 12 h, the mice were sacrificed, and tissues were embedded in paraffin and analyzed by immunohistochemistry.

**Histological Analysis and Immunohistochemistry.** Excised tissues were fixed in 4% paraformaldehyde at 4 °C overnight, dehydrated with ethanol, and then embedded in paraffin. Tissues were sectioned with a thickness of 4 $\mu$m, deparaffinized with xylene, hydrated with ethanol and water, and stained with hematoxylin and eosin (H&E) or terminal deoxyribonucleotidyl transferase (TdT)-mediated biotin-16-dUTP nick-end labeling (TUNEL). Images were acquired using an Olympus BX51 microscope.

For immunohistochemistry, deparaffinized tissues were blocked with 5% horse serum/0.02% Triton X-100 in TBS for 2 h and incubated overnight at 4 °C with anti-CD31 (Santa Cruz Biotechnology), anti-phosphohistone 3 (Upstate Biotechnology), anti-ICAM-1 antibodies (R&D Systems). After treatment with Alexa Fluor-conjugated secondary antibodies for 2 h at room temperature, cells were counterstained with Hoechst for 10 min. Images were acquired using an Olympus FV1000 microscope. For evaluation of the CD31-positive area on tumor tissue, 10 images were randomly obtained from five independent tumor sections. The CD31-positive area was quantified using ImageJ software (http://rsb.info.nih.gov/ij/). For phosphohistone-3-positive cells, 10 areas were randomly imaged, and live cells were counted using MetaMorph software.

**Statistical Analysis.** Statistical analysis was performed using GraphPad Prism software (GraphPad Software). *In vitro* and *in vivo* data are shown as the mean ± SD and mean ± SEM, respectively. *P*-values were calculated using the unpaired two-tailed Student's *t* test. Tumor volume measurement experiments were analyzed using the paired two-tailed Student's *t* test. $P < 0.05$ was considered to be significant.

*Conflict of Interest:* The authors declare the following competing financial interest(s): S.C.J., O.Y.K., D.-S.C., Y.-K.K., and Y.S.G. are the inventors of a patent relating to the use of artificial nanovesicles for delivery vehicles (International Application No.: PCT/KR2010/004277; Publication Date: 01.07.2010). All rights have been assigned to Aeon Medix.

*Acknowledgment.* This work was supported by the Midcareer Researcher Program through an NRF grant funded by the MEST (No. 2013035248) and a grant of the Korea Healthcare Technology R&D Project, Ministry for Health and Welfare, Republic of Korea (A092258 and A120273).

*Supporting Information Available:* Additional figures and table as described in the text. This material is available free of charge *via* the Internet at http://pubs.acs.org.

## REFERENCES AND NOTES

1. Hanahan, D.; Weinberg, R. A. Hallmarks of Cancer: The Next Generation. *Cell* **2011**, *144*, 646–674.
2. Halazonetis, T. D.; Gorgoulis, V. G.; Bartek, J. An Oncogene-Induced DNA Damage Model for Cancer Development. *Science* **2008**, *319*, 1352–1355.
3. Michod, D.; Widmann, C. DNA-Damage Sensitizers: Potential New Therapeutical Tools to Improve Chemotherapy. *Crit. Rev. Oncol. Hematol.* **2007**, *63*, 160–171.
4. Jackson, S. P.; Bartek, J. The DNA-Damage Response in Human Biology and Disease. *Nature* **2009**, *461*, 1071–1078.
5. Schiff, D.; Wen, P. Y.; van den Bent, M. J. Neurological Adverse Effects Caused by Cytotoxic and Targeted Therapies. *Nat. Rev. Clin. Oncol.* **2009**, *6*, 596–603.
6. Lian, T.; Ho, R. J. Trends and Developments in Liposome Drug Delivery Systems. *J. Pharm. Sci.* **2001**, *90*, 667–680.
7. Peer, D.; Karp, J. M.; Hong, S.; Farokhzad, O. C.; Margalit, R.; Langer, R. Nanocarriers as an Emerging Platform for Cancer Therapy. *Nat. Nanotechnol.* **2007**, *2*, 751–760.
8. Farokhzad, O. C.; Langer, R. Impact of Nanotechnology on Drug Delivery. *ACS Nano* **2009**, *3*, 16–20.
9. Murphy, E. A.; Majeti, B. K.; Barnes, L. A.; Makale, M.; Weis, S. M.; Lutu-Fuga, K.; Wrasidlo, W.; Cheresh, D. A. Nanoparticle-Mediated Drug Delivery to Tumor Vasculature Suppresses Metastasis. *Proc. Natl. Acad. Sci. U. S. A.* **2008**, *105*, 9343–9348.
10. Yang, H.; Tyagi, P.; Kadam, R. S.; Holden, C. A.; Kompella, U. B. Hybrid Dendrimer Hydrogel/PLGA Nanoparticle Platform Sustains Drug Delivery for One Week and Antiglaucoma Effects for Four Days Following One-Time Topical Administration. *ACS Nano* **2012**, *6*, 7595–7606.
11. Stefanick, J. F.; Ashley, J. D.; Kiziltepe, T.; Bilgicer, B. A Systematic Analysis of Peptide Linker Length and Liposomal Polyethylene Glycol Coating on Cellular Uptake of Peptide-Targeted Liposomes. *ACS Nano* **2013**, *7*, 2935–2947.
12. Davis, M. E.; Chen, Z. G.; Shin, D. M. Nanoparticle Therapeutics: An Emerging Treatment Modality for Cancer. *Nat. Rev. Drug Discovery* **2008**, *7*, 771–782.
13. Maeda, H.; Wu, J.; Sawa, T.; Matsumura, Y.; Hori, K. Tumor Vascular Permeability and the EPR Effect in Macromolecular Therapeutics: A Review. *J. Controlled Release* **2000**, *65*, 271–284.
14. Ferrari, M. Nanogeometry: Beyond Drug Delivery. *Nat. Nanotechnol.* **2008**, *3*, 131–132.
15. Thery, C.; Ostrowski, M.; Segura, E. Membrane Vesicles as Conveyors of Immune Responses. *Nat. Rev. Immunol.* **2009**, *9*, 581–593.
16. Sharma, S.; Rasool, H. I.; Palanisamy, V.; Mathisen, C.; Schmidt, M.; Wong, D. T.; Gimzewski, J. K. Structural-Mechanical Characterization of Nanoparticle Exosomes in Human Saliva, Using Correlative AFM, FESEM, and Force Spectroscopy. *ACS Nano* **2010**, *4*, 1921–1926.
17. Kim, D. K.; Kang, B.; Kim, O. Y.; Choi, D. S.; Lee, J.; Kim, S. R.; Go, G.; Yoon, Y. J.; Kim, J. H.; Jang, S. C.; et al. EVpedia: An Integrated Database of High-Throughput Data for Systemic Analyses of Extracellular Vesicles. *J. Extracell. Vesicles* **2013**, *2*, 20384.
18. Ratajczak, J.; Wysoczynski, M.; Hayek, F.; Janowska-Wieczorek, A.; Ratajczak, M. Z. Membrane-Derived Microvesicles: Important and Underappreciated Mediators of Cell-to-Cell Communication. *Leukemia* **2006**, *20*, 1487–1495.
19. Valadi, H.; Ekstrom, K.; Bossios, A.; Sjostrand, M.; Lee, J. J.; Lotvall, J. O. Exosome-Mediated Transfer of mRNAs and MicroRNAs Is a Novel Mechanism of Genetic Exchange Between Cells. *Nat. Cell Biol.* **2007**, *9*, 654–659.

20. Skog, J.; Wurdinger, T.; van Rijn, S.; Meijer, D. H.; Gainche, L.; Sena-Esteves, M.; Curry, W. T., Jr.; Carter, B. S.; Krichevsky, A. M.; Breakefield, X. O. Glioblastoma Microvesicles Transport RNA and Proteins That Promote Tumour Growth and Provide Diagnostic Biomarkers. *Nat. Cell Biol.* **2008**, *10*, 1470–1476.
21. Hong, B. S.; Cho, J. H.; Kim, H.; Choi, E. J.; Rho, S.; Kim, J.; Kim, J. H.; Choi, D. S.; Kim, Y. K.; Hwang, D.; et al. Colorectal Cancer Cell-Derived Microvesicles Are Enriched in Cell Cycle-Related mRNAs That Promote Proliferation of Endothelial Cells. *BMC Genomics* **2009**, *10*, 556.
22. Choi, D. S.; Lee, J. M.; Park, G. W.; Lim, H. W.; Bang, J. Y.; Kim, Y. K.; Kwon, K. H.; Kwon, H. J.; Kim, K. P.; Gho, Y. S. Proteomic Analysis of Microvesicles Derived from Human Colorectal Cancer Cells. *J. Proteome Res.* **2007**, *6*, 4646–4655.
23. Zhuang, X.; Xiang, X.; Grizzle, W.; Sun, D.; Zhang, S.; Axtell, R. C.; Ju, S.; Mu, J.; Zhang, L.; Steinman, L.; et al. Treatment of Brain Inflammatory Diseases by Delivering Exosome Encapsulated Anti-Inflammatory Drugs from the Nasal Region to the Brain. *Mol. Ther.* **2011**, *19*, 1769–1779.
24. Sun, D.; Zhuang, X.; Xiang, X.; Liu, Y.; Zhang, S.; Liu, C.; Barnes, S.; Grizzle, W.; Miller, D.; Zhang, H. G. A Novel Nanoparticle Drug Delivery System: The Anti-Inflammatory Activity of Curcumin Is Enhanced When Encapsulated in Exosomes. *Mol. Ther.* **2010**, *18*, 1606–1614.
25. Alvarez-Erviti, L.; Seow, Y.; Yin, H.; Betts, C.; Lakhal, S.; Wood, M. J. Delivery of siRNA to the Mouse Brain by Systemic Injection of Targeted Exosomes. *Nat. Biotechnol.* **2011**, *29*, 341–345.
26. Wahlgren, J.; De, L. K. T.; Brisslert, M.; Vaziri Sani, F.; Telemo, E.; Sunnerhagen, P.; Valadi, H. Plasma Exosomes Can Deliver Exogenous Short Interfering RNA to Monocytes and Lymphocytes. *Nucleic Acids Res.* **2012**, *40*, e130.
27. van Dommelen, S. M.; Vader, P.; Lakhal, S.; Kooijmans, S. A.; van Solinge, W. W.; Wood, M. J.; Schiffelers, R. M. Microvesicles and Exosomes: Opportunities for Cell-Derived Membrane Vesicles in Drug Delivery. *J. Controlled Release* **2012**, *161*, 635–644.
28. Lakhal, S.; Wood, M. J. Exosome Nanotechnology: An Emerging Paradigm Shift in Drug Delivery: Exploitation of Exosome Nanovesicles for Systemic *in Vivo* Delivery of RNAi Heralds New Horizons for Drug Delivery Across Biological Barriers. *Bioessays* **2011**, *33*, 737–741.
29. Choi, D. S.; Kim, D. K.; Kim, Y. K.; Gho, Y. S. Proteomics, Transcriptomics and Lipidomics of Exosomes and Ectosomes. *Proteomics* **2013**, *13*, 1554–1571.
30. Shedden, K.; Xie, X. T.; Chandaroy, P.; Chang, Y. T.; Rosania, G. R. Expulsion of Small Molecules in Vesicles Shed by Cancer Cells: Association with Gene Expression and Chemosensitivity Profiles. *Cancer Res.* **2003**, *63*, 4331–4337.
31. Ley, K.; Laudanna, C.; Cybulsky, M. I.; Nourshargh, S. Getting to the Site of Inflammation: The Leukocyte Adhesion Cascade Updated. *Nat. Rev. Immunol.* **2007**, *7*, 678–689.
32. Lee, H. M.; Choi, E. J.; Kim, J. H.; Kim, T. D.; Kim, Y. K.; Kang, C.; Gho, Y. S. A Membranous Form of ICAM-1 on Exosomes Efficiently Blocks Leukocyte Adhesion to Activated Endothelial Cells. *Biochem. Biophys. Res. Commun.* **2010**, *397*, 251–256.
33. Mackay, F.; Loetscher, H.; Stueber, D.; Gehr, G.; Lesslauer, W. Tumor Necrosis Factor Alpha (TNF-Alpha)-Induced Cell Adhesion to Human Endothelial Cells Is Under Dominant Control of One TNF Receptor Type, TNF-R55. *J. Exp. Med.* **1993**, *177*, 1277–1286.
34. Zhou, S.; Starkov, A.; Froberg, M. K.; Leino, R. L.; Wallace, K. B. Cumulative and Irreversible Cardiac Mitochondrial Dysfunction Induced by Doxorubicin. *Cancer Res.* **2001**, *61*, 771–777.
35. Yoong, K. F.; McNab, G.; Hubscher, S. G.; Adams, D. H. Vascular Adhesion Protein-1 and ICAM-1 Support the Adhesion of Tumor-Infiltrating Lymphocytes to Tumor Endothelium in Human Hepatocellular Carcinoma. *J. Immunol.* **1998**, *160*, 3978–3988.
36. Palazon, A.; Teijeira, A.; Martinez-Forero, I.; Hervas-Stubbs, S.; Roncal, C.; Penuelas, I.; Dubrot, J.; Morales-Kastresana, A.; Perez-Gracia, J. L.; Ochoa, M. C.; et al. Agonist Anti-CD137 mAb Act on Tumor Endothelial Cells to Enhance Recruitment of Activated T Lymphocytes. *Cancer Res.* **2011**, *71*, 801–811.
37. Ferrara, N.; Kerbel, R. S. Angiogenesis as a Therapeutic Target. *Nature* **2005**, *438*, 967–974.
38. Weis, S. M.; Cheresh, D. A. Tumor Angiogenesis: Molecular Pathways and Therapeutic Targets. *Nat. Med.* **2011**, *17*, 1359–1370.
39. Kim, C. W.; Lee, H. M.; Lee, T. H.; Kang, C.; Kleinman, H. K.; Gho, Y. S. Extracellular Membrane Vesicles from Tumor Cells Promote Angiogenesis via Sphingomyelin. *Cancer Res.* **2002**, *62*, 6312–6317.
40. Yoon, Y. J.; Chang, S.; Kim, O. Y.; Kang, B. K.; Park, J.; Lim, J. H.; Huang, J. Y.; Kim, Y. K.; Byun, J. H.; Gho, Y. S. Three-Dimensional Imaging of Hepatic Sinusoids in Mice Using Synchrotron Radiation Micro-Computed Tomography. *PLoS ONE* **2013**, *8*, e68600.
41. Johnston, S. C.; Dustin, M. L.; Hibbs, M. L.; Springer, T. A. On the Species Specificity of the Interaction of LFA-1 with Intercellular Adhesion Molecules. *J. Immunol.* **1990**, *145*, 1181–1187.
42. Terry, R. W.; Kwee, L.; Levine, J. F.; Labow, M. A. Cytokine Induction of an Alternatively Spliced Murine Vascular Cell Adhesion Molecule (VCAM) mRNA Encoding a Glycosylphosphatidylinositol-Anchored VCAM Protein. *Proc. Natl. Acad. Sci. U. S. A.* **1993**, *90*, 5919–5923.
43. Huo, Y.; Hafezi-Moghadam, A.; Ley, K. Role of Vascular Cell Adhesion Molecule-1 and Fibronectin Connecting Segment-1 in Monocyte Rolling and Adhesion on Early Atherosclerotic Lesions. *Circ. Res.* **2000**, *87*, 153–159.
44. You, Y.; Duan, Y.; Liu, S. W.; Zhang, X. L.; Feng, J. T.; Yan, C. H.; Han, Y. L. Anti-Atherosclerotic Function of Astragali Radix Extract: Downregulation of Adhesion Molecules *in Vitro* and *in Vivo*. *BMC Complementary Altern. Med.* **2012**, *12*, 54.
45. Choi, J.; Woo, H. N.; Ju, E. J.; Jung, J.; Chung, H. K.; Park, J.; Park, S. S.; Shin, S. H.; Park, H. J.; Lee, J. S.; et al. Immunocytes as a Biocarrier to Delivery Therapeutic and Imaging Contrast Agents to Tumors. *J. Nanomater.* **2012**, *2012*, 863704.
46. Carmeliet, P.; Jain, R. K. Angiogenesis in Cancer and Other Diseases. *Nature* **2000**, *407*, 249–257.
47. Ohno, S.; Takanashi, M.; Sudo, K.; Ueda, S.; Ishikawa, A.; Matsuyama, N.; Fujita, K.; Mizutani, T.; Ohgi, T.; Ochiya, T.; et al. Systemically Injected Exosomes Targeted to EGFR Deliver Antitumor MicroRNA to Breast Cancer Cells. *Mol. Ther.* **2013**, *21*, 185–191.
48. Lee, D. E.; Koo, H.; Sun, I. C.; Ryu, J. H.; Kim, K.; Kwon, I. C. Multifunctional Nanoparticles for Multimodal Imaging and Theragnosis. *Chem. Soc. Rev.* **2012**, *41*, 2656–2672.
49. Sanson, C.; Diou, O.; Thevenot, J.; Ibarboure, E.; Soum, A.; Brulet, A.; Miraux, S.; Thiaudiere, E.; Tan, S.; Brisson, A.; et al. Doxorubicin Loaded Magnetic Polymersomes: Theranostic Nanocarriers for MR Imaging and Magneto-Chemotherapy. *ACS Nano* **2011**, *5*, 1122–1140.
50. Gho, Y. S.; Kleinman, H. K.; Sosne, G. Angiogenic Activity of Human Soluble Intercellular Adhesion Molecule-1. *Cancer Res.* **1999**, *59*, 5128–5132.
51. Liu, C.; Yu, S.; Zinn, K.; Wang, J.; Zhang, L.; Jia, Y.; Kappes, J. C.; Barnes, S.; Kimberly, R. P.; Grizzle, W. E.; et al. Murine Mammary Carcinoma Exosomes Promote Tumor Growth by Suppression of NK Cell Function. *J. Immunol.* **2006**, *176*, 1375–1385.
52. Lowery, A.; Onishko, H.; Hallahan, D. E.; Han, Z. Tumor-Targeted Delivery of Liposome-Encapsulated Doxorubicin by Use of a Peptide That Selectively Binds to Irradiated Tumors. *J. Controlled Release* **2011**, *150*, 117–124.
53. Veldman, R. J.; Koning, G. A.; van Hell, A.; Zerp, S.; Vink, S. R.; Storm, G.; Verheij, M.; van Blitterswijk, W. J. Coformulated N-Octanoyl-Glucosylceramide Improves Cellular Delivery and Cytotoxicity of Liposomal Doxorubicin. *J. Pharmacol. Exp. Ther.* **2005**, *315*, 704–710.

54. Sun, J.; Blaskovich, M. A.; Knowles, D.; Qian, Y.; Ohkanda, J.; Bailey, R. D.; Hamilton, A. D.; Sebti, S. M. Antitumor Efficacy of a Novel Class of Non-Thiol-Containing Peptidomimetic Inhibitors of Farnesyltransferase and Geranylgeranyltransferase I: Combination Therapy with the Cytotoxic Agents Cisplatin, Taxol, and Gemcitabine. *Cancer Res.* **1999**, *59*, 4919–4926.